AD-A111 606 WISCONSIN UNIV-MADISON DEPT OF ELECTRICAL AND COMPUT--ETC F/G 9/3
IN-SITU MICROWAVE MEASUREMENTS OF LOSSY DIELECTRICS.(U)
JAN 82 R J KING, C D KIM, J B BEYER DAAG29-80-C-0106
UNCLASSIFIED ECE-82-1 ARO-15586.1-MS NL

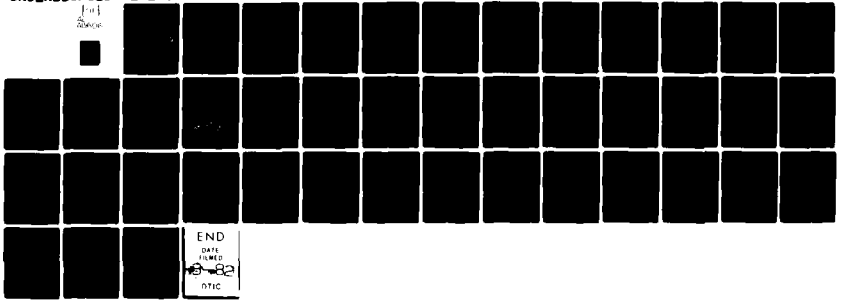

END
DATE FILMED
4-82
DTIC

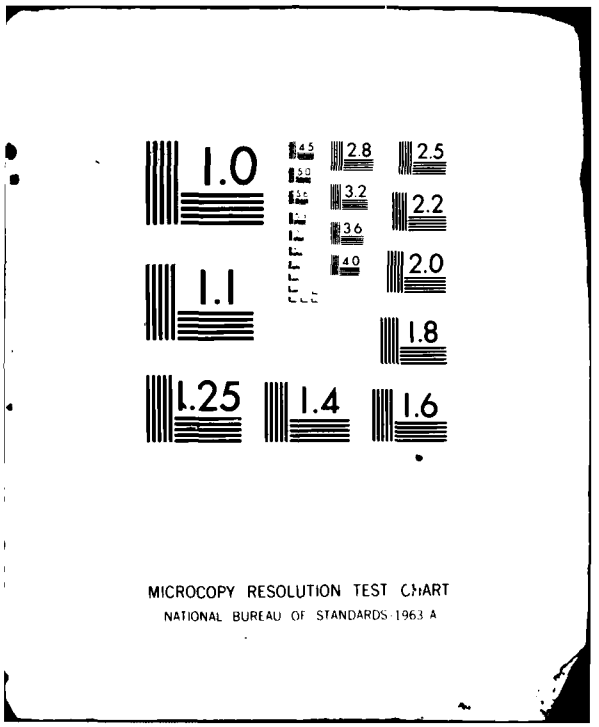

ARO 15586.1-GS

Electrical

Computer

Engineering

DEPARTMENT OF ELECTRICAL
AND COMPUTER ENGINEERING

UNIVERSITY OF WISCONSIN-MADISON

ECE-82-1 January 1982

IN-SITU MICROWAVE MEASUREMENTS OF LOSSY DIELECTRICS

R. J. King
C. D. Kim
J. B. Beyer

Department of Electrical & Computer Engineering
University of Wisconsin
Madison, WI 53706

ENGINEERING EXPERIMENT STATION
MADISON, WISCONSIN 53706

SECURITY CLASSIFICATION OF THIS PAGE *(When Data Entered)*

REPORT DOCUMENTATION PAGE

READ INSTRUCTIONS BEFORE COMPLETING FORM

1. REPORT NUMBER: ECE-82-1	2. GOVT ACCESSION NO.
3. RECIPIENT'S CATALOG NUMBER	
4. TITLE *(and Subtitle)*: IN-SITU MICROWAVE MEASUREMENTS OF LOSSY DIELECTRICS	5. TYPE OF REPORT & PERIOD COVERED: Final Report 9/15/78 through 1/15/82
	6. PERFORMING ORG. REPORT NUMBER
7. AUTHOR(s): R. J. King, C. D. Kim and J. B. Beyer	8. CONTRACT OR GRANT NUMBER(s): DAAG 29-78-G-0181 DAAG 29-80-C-0106
9. PERFORMING ORGANIZATION NAME AND ADDRESS: Department of Electrical and Computer Engineering, University of Wisconsin, Madison, WI 53706	10. PROGRAM ELEMENT, PROJECT, TASK AREA & WORK UNIT NUMBERS
11. CONTROLLING OFFICE NAME AND ADDRESS: U.S. Army Research Office, P.O. Box 12211, Research Triangle Park, NC 27709	12. REPORT DATE: January 1982
	13. NUMBER OF PAGES: 39
14. MONITORING AGENCY NAME & ADDRESS *(if different from Controlling Office)*: Office of Naval Research Branch Office, 536 South Clark Street, Chicago, IL 60605	15. SECURITY CLASS. *(of this report)*: Unclassified
	15a. DECLASSIFICATION/DOWNGRADING SCHEDULE: N/A

16. DISTRIBUTION STATEMENT *(of this Report)*

Approved for public release; distribution unlimited.

17. DISTRIBUTION STATEMENT *(of the abstract entered in Block 20, if different from Report)*

NA

18. SUPPLEMENTARY NOTES

1. Presented, in part, at the 1979 National Radio Science Meeting, 18-22 June, Seattle, Washington.
2. The findings in this report are not to be construed as an official Department of the Army position, unless so designated by other authorized documents.

19. KEY WORDS *(Continue on reverse side if necessary and identify by block number)*

Microwave Measurements
Dielectric Constant (Complex)
Homodyne Detection
In-Situ Measurements
Propagation Constant (of Traveling Wave)
Modulated Scatterers
Remote Sensing

20. ABSTRACT *(Continue on reverse side if necessary and identify by block number)*

The objective of this work has been to develop microwave (4.9 GHz) instrumentation systems, and measurement and inversion techniques for determining the complex dielectric constant of lossy media in-situ. Unique features of this work, compared to other studies, are that the complex propagation constants of traveling waves which are coupled to the medium under test are measured using phase-sensitive homodyne systems.

An invasive method was studied wherein a small modulated scattering probe is inserted into a test hole in the medium, and the propagation constant

DD FORM 1 JAN 73 1473 EDITION OF 1 NOV 65 IS OBSOLETE

Unclassified

SECURITY CLASSIFICATION OF THIS PAGE *(When Data Entered)*

20. (continued)

of a spherically expanding wave originating outside the medium is measured. Results are given for portage sand vs moisture content.

A non-invasive method uses an open-walled slotted rectangular waveguide laid directly on the surface to couple the traveling wave in the waveguide to the medium. The instrumentation and measurement techniques work quite well and results are given for several media, e.g., rock, concrete, sand, etc. A promising inversion method for finding the dielectric constant is presented, along with suggested improvements in the design of the traveling wave applicator and the detection instrumentation.

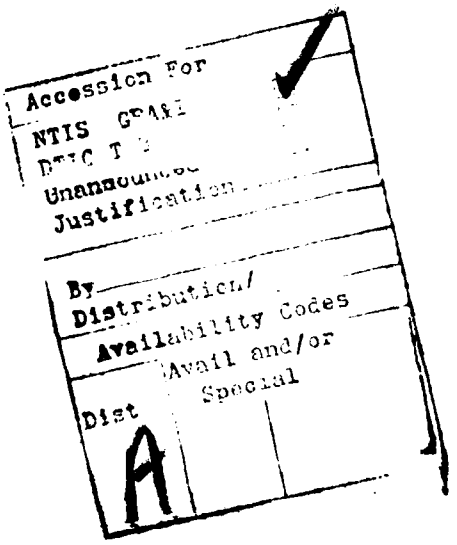

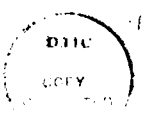

IN-SITU MICROWAVE MEASUREMENTS OF LOSSY DIELECTRICS

Final Report

R. J. King
C. D. Kim
J. B. Beyer

January 1982

US Army Research Office

Contract/Grant No.
DAAG29-78-G-0181
DAAG29-80-C-0106

Department of Electrical and Computer Engineering
University of Wisconsin
Madison, WI 53706

ECE-82-1

Approved for Public Release:
Distribution Unlimited

IN-SITU MICROWAVE MESUREMENTS OF LOSSY DIELECTRICS

R. J. King, C. D. Kim and J. B. Beyer
Department of Electrical and Computer Engineering
University of Wisconsin, Madison, WI 53706

INTRODUCTION

The prime objective of this work has been to develop mic... instrumentation systems, and measurement and inversion techniques ... determining the complex dielectric constant of lossy media in-s tu. ... commonly used methods are not in-situ, e.g., laboratory methods requir... removing the sample from location and preparing it for testing b... and fitting it into a waveguide, cavity, etc. Such preparation can sig ficant y alter the electrical properties by changing the density, releasing stress and/or changing the moisture content. Other in-situ methods rely on the reflection of the wave from the surface of the medium. These methods given reasonable accuracy for low-loss media, but the accuracy suffers when the medium has a large complex dielectric constant, especially when the loss tangent is not small compared to unity.

Unique features of this work, compared to other studies, are that the complex propagation constants ($\gamma = \alpha+j\beta$) of traveling waves are measured using phase-sensitive homodyne instrumentation systems. This phase-sensit v... property permits measuring the variations of the phase as well as the amplitude of the propagating field. Homodyne systems are well known for their linearity, extremely good sensitivity and great dynamic range.

The relationship between the complex propagation constant, γ, and the complex dielectric constant ε ($= \varepsilon'-j\varepsilon''$) is determined by the method used to couple the electromagnetic field with the medium. These coupling methods and the solutions of the corresponding inversion problems to find ε are the main topics of this work.

An invasive method and a non-invasive method were studied. In the invasive method, a small modulated scattering probe is inserted into a test

hole in the medium. When the medium is illuminated by a spherically expanding wave originating from a horn source outside the medium, the complex propagation constant, γ, is measured. After correcting for spherical expansion, ε can be calculated in a straightforward manner. Another advantage of this methid is that $\gamma(z)$ can be measured, and hence $\varepsilon(z)$ can be found, for materials which are graded gradually in the direction normal to the surface. The chief disadvantage of the method is that a hole is required. The dielectric constant of Portage sand with various moisture contents were measured.

The non-invasive method uses an open-walled rectangular waveguide laid on the surface to couple the traveling wave in the waveguide with the medium. The instrumentation and techniques for measuring γ for the traveling wave work quite well, but the task of inverting the data to find ε is difficult owing to the complicated boundary value problem which must be formulated and solved. An approximate solution has been obtained which correctly shows the general trends, but further work is needed to attain reasonable accuracy. Results are given for several materials such as sand, rock and concrete. Besides improving the approximations in the analysis, a particularly promising improvement in the apparatus entails filling the waveguide with a low-loss dielectric such that the dielectric constant of the medium, relative to that in the waveguide, is scaled down. This has the additional advantage of reducing the size of applicator waveguide.

Further studies are suggested which use two-conductor traveling wave applicators for coupling the wave to the medium. The advantage of these, compared to the rectangular waveguide, is that the operating bandwidth is substantially increased. Other instrumentation improvements are suggested for increasing the sensitivity, dynamic range, accuracy and ease of use.

I. THE MICROWAVE HOMODYNE SYSTEM

In this work, a microwave homodyne system has been used to measure the attenuation and phase of the field to obtain the complex propagation constant γ ($=\alpha+j\beta$), from which the complex dielectric constant of the medium can be found.

First, the basic principles of the instrumentation as shown in Fig. 1 are described briefly. Further details on homodyne systems in general are given in the book by King [1978].

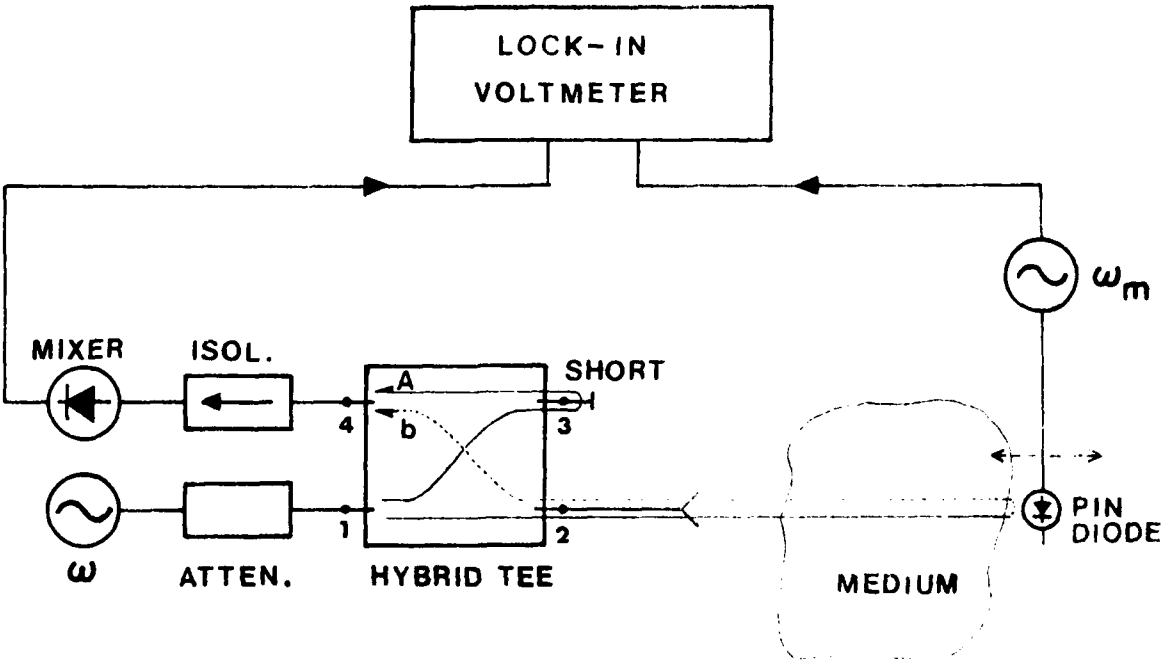

Fig. 1. Microwave homodyne system for measuring the complex propagation constant of a traveling wave.

The output of the CW microwave (200 mW at 4.9 GHz) source is split at port 1 and fed into the two channels: the reference channel and the information channel. The CW reference signal, A, of 6 - 10 dBm is derived by

reflection from a short at port 3 as shown by the solid signal flow path. This level is sufficient to ensure that the mixer operates as a linear detector. The short at port 3 can be moved to vary the phase of the reference signal, A, although its position is generally fixed in actual operation.

In the information channel, the CW signal which passes from port 2 propagates through the unknown medium and is backscattered by a modulated scatterer which actually is a small dipole (electric or magnetic), switched at the audio angular frequency ω_m (f_m = 10 KHz). The double sideband amplitude modulated (DSBAM) backscattered signal, b, is fed into the mixer via port 2 and port 4, as shown by the dashed signal flow path. This modulated signal at the mixer is of the form

$$|b|[1 + m \cos(\omega_m t)]\cos(\omega t+\phi) \qquad (1)$$

where m is the amplitude modulation index and ϕ is the phase difference between the reference signal and the backscattered signal.

The detected homodyne output signal at ω_m is given by

$$e_{out} \tilde{=} K_h |b| m \cos(\phi) \cos(\omega_m t) \quad \text{for } b/A \ll 1 \qquad (2)$$

where K_h is the mixer conversion constant.

Thus, the variation of amplitude $|b|$ and phase ϕ can be measured as functions of the position of the modulated scattering probe. This information is then used to directly determine the propagation constant γ of a traveling wave, owing to the phase sensitive nature of homodyne detection. In contrast, a long-standing indirect technique for measuring γ has been to create a standing wave in the field which is coupled to the medium and to use video detection to measure the standing wave pattern. But if the losses of the medium are appreciable, the minima of the pattern are not sharp and spaced a

half wavelength apart. It then becomes necessary to analyze the data graphically or by computer to find α and β [Gardoil, 1975]. Furthermore, it is not always possible to create a standing wave in the medium in-situ.

This study uses the phase sensitive property of homodyne detection throughout to measure γ of various traveling waves which are coupled to the medium under investigation.

II. MEASUREMENT METHODS

Two different methods, an invasive method and a non-invasive method, were studied to determine the complex dielectric constant.

1. The Invasive Method

In the invasive method, the complex propagation constant of a spherically expanding wave propagating in the medium is measured by inserting a modulated probe into the medium, as shown in Fig. 2.

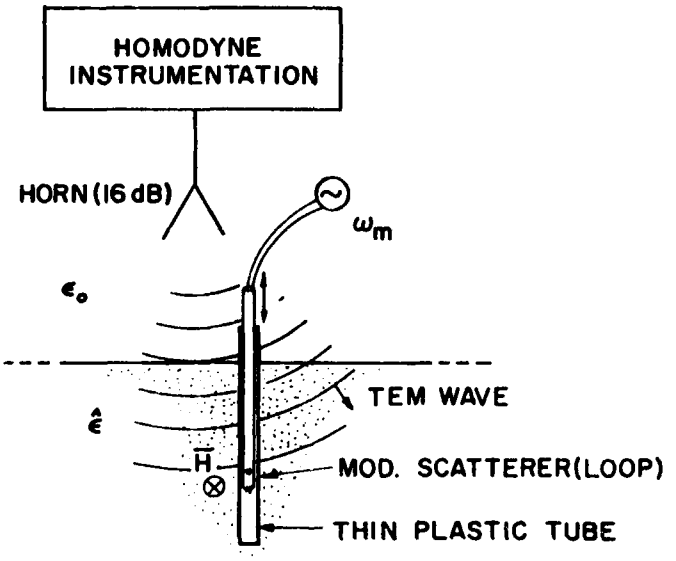

Fig. 2. Measurement set up for the invasive method.

The probe is a small loop terminated with two PIN diodes which are switched at 10 KHz via resistive leads, as shown in Fig. 3.

The TEM wave is launched by a horn antenna, and propagates perpendicular to the surface of the medium. The magnetic field inside the medium is a spherically expanding wave

$$H = H_0 \frac{e^{-\gamma z}}{z}$$
$$= H_0 \left(\frac{e^{-\alpha z}}{z}\right) e^{-j\beta z} \qquad (3)$$

where z is assumed to be in the radiation zone.

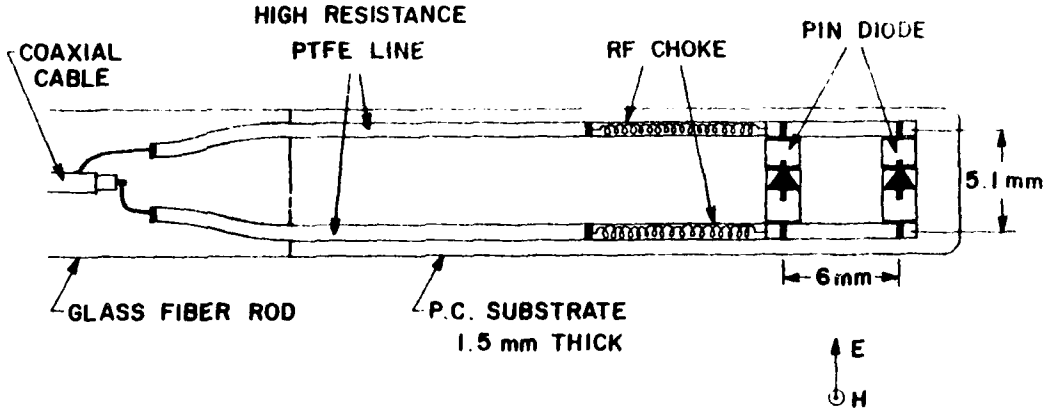

Fig. 3. Modulated loop scatterer.

Then the backscattered signal, b, which is proportional to the square of the incident field at the scatterer [King, 1978] is of the form

$$b = b_0 \frac{e^{-2\alpha z}}{z^2} e^{-j2\beta z} \qquad (4)$$

Thus, from (2), the amplitude of the homodyne output at ω_m is

$$V_{out} \tilde{=} K_h |b| m \cos(\phi)$$
$$= V_0 \frac{e^{-2\alpha z}}{z^2} \cos(2\beta z) \qquad (5)$$

Therefore, to get α the effect of the z^{-2} spreading factor must be corrected. To do this requires determining the effective origin of the horn antenna. This can be done by matching the measured intensity versus distance curve for free space with the z^{-2} curve.

The factor of $\cos(2\beta z)$ gives zero crossings for every quarter-wavelength in the medium. Thus, β can be easily calculated by measuring the distance between zeros. In practice, several zeros are traversed, and the results averaged.

A typical plot of (5) which pertains to the field in wet Portage sand is shown in Fig. 4.

The moisture content of the uppermost sand is relatively constant with depth. However, as the water tends to settle the moisture content increases sharply at a depth of about 8 cm, such that the space between the sand particles is filled with water. Thereafter, the moisture content does not increase further. The wave attenuation therefore increases sharply at the boundary where the sand is saturated with water, as shown by the amplitude of the last two peaks in Fig. 4.

The relation between the dielectric constant, ε, and α and β is

$$\begin{aligned} \beta - j\alpha &= \omega\sqrt{\mu\varepsilon} \\ &= k_0 \sqrt{\varepsilon_r} \end{aligned} \tag{6}$$

for non-magnetic material where k_0 is the wave number of free space.

Thus,

$$\begin{aligned} \varepsilon_r &= \varepsilon_r' - j\varepsilon_r'' \\ &= \frac{1}{k_0^2} (\beta - j\alpha)^2 \end{aligned} \tag{7}$$

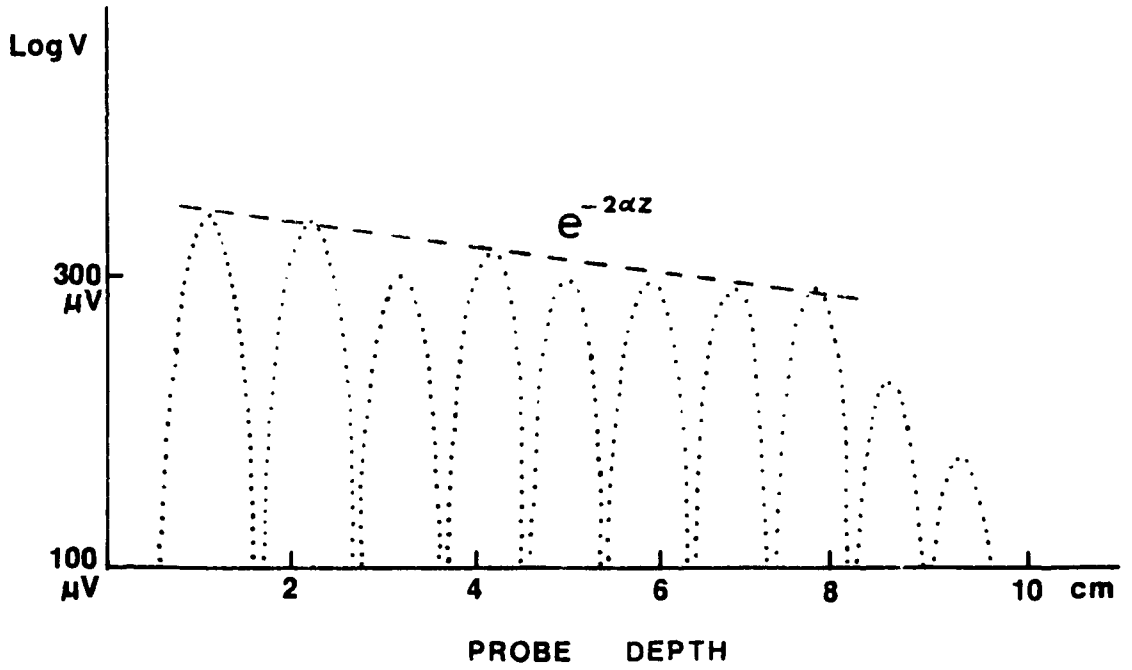

Fig. 4. Typical output of the homodyne system

or,

$$\epsilon_r' = (\beta^2-\alpha^2)/k_0^2 \tag{8a}$$

$$\epsilon_r'' = 2\alpha\beta/k_0^2 \tag{8b}$$

Several measurement were made on Portage sand with various moisture contents. The results are shown in Fig. 5. The moisture content used in this measurement is defined by

$$\theta_w = \frac{\text{mass of the water contained}}{\text{mass of dry sand}} \times 100\%$$

The disadvantages of this method are:

a) For solids, it requires drilling a hole into the medium.

b) For a dielectric medium the effective origin of the horn is changed by refraction. To reduce this effect on the attenuation, the horn must be located several wavelengths from tne surface of the medium.

c) The presence of the plastic tube and the glass fiber rod on which the scatterer is mounted may affect the propagation constant being measured.

The chief advantage of this method is that the inversion from the measured propagation constant, γ, to the dielectric constant, ε, is quite straightforward assuming a TEM wave. Another advantage is that slow variations of $\gamma(z)$ and hence $\varepsilon(z)$ can be measured versus depth.

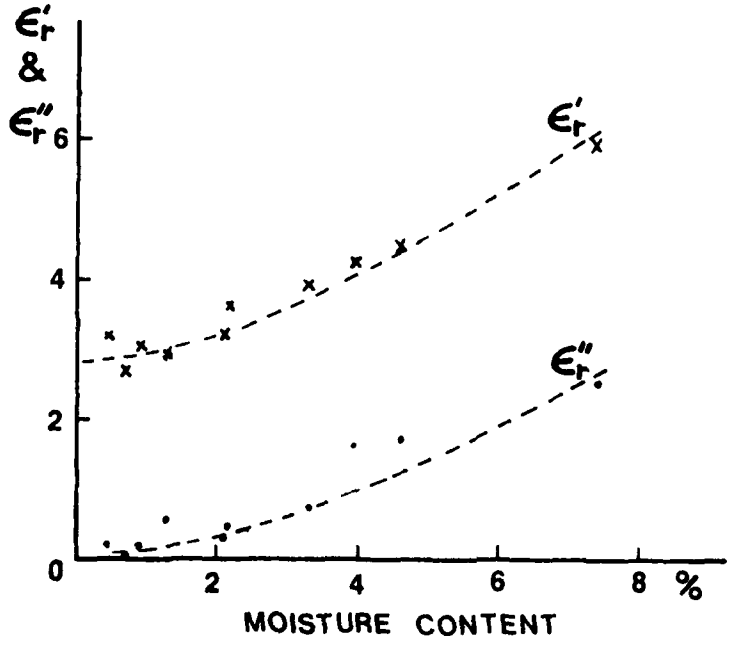

Fig. 5. ε_r' and ε_r'' vs moisture content for Portage sand.

2. The Non-Invasive Method

This method uses a slotted open-walled rectangular waveguide laid directly on the surface, as shown in Figs. 6, 7 & 8. The longitudinal propagation constant of a traveling wave which is coupled to the unknown medium is measured. Again, a modulated scatterer and homodyne detection are used to probe the field of the traveling wave.

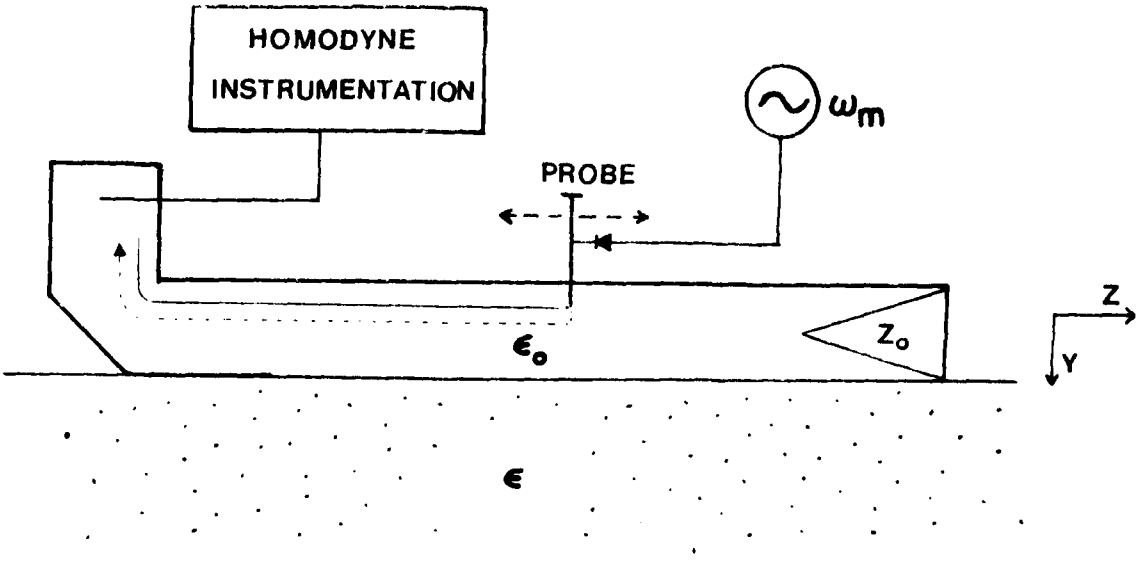

Fig. 6. Measurement system for the non-invasive method.

A TE_{10} mode propagates toward the right in the closed portion of the waveguide in Figs. 6 and 7. In the open portion, this wave is converted into a traveling leaky waveguide mode, where the fields are coupled to the unknown medium. The right end of the waveguide in Figs. 6 and 7 is terminated with Z_0 to minimize the reflection. The top wall of the waveguide is slotted longitudinally and an electrically modulated slotted line probe is inserted to scatter the incoming traveling wave. In a reciprocal manner, the backscattered wave propagates back to the homodyne instrumentation where it is detected.

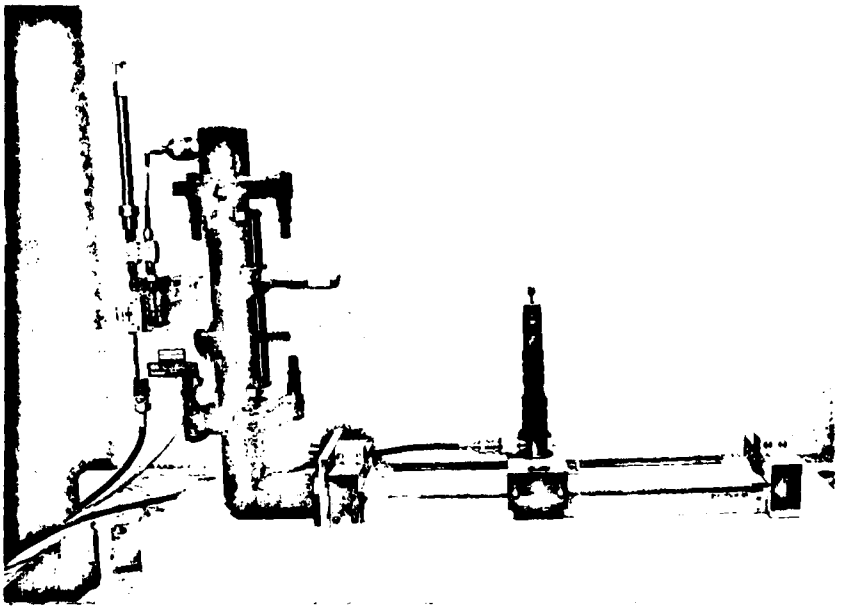

Fig. 7. Microwave apparatus for the non-invasive method.

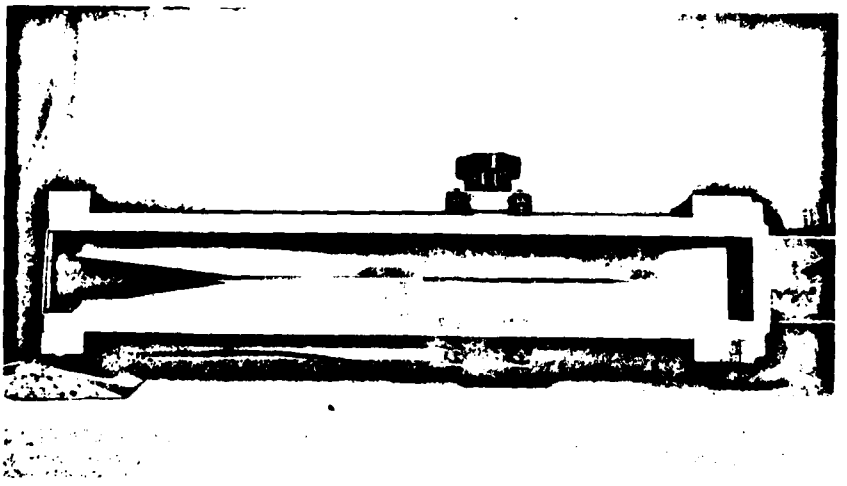

Fig. 8. Bottom view of open-walled waveguide. The TE_{10} mode waveguide feed is on right side, and the Z_0 termination is on the left side.

Since the bottom wall is removed, the inside dimension (1.872 × 0.936 inches) of the open-walled waveguide is same in width and slightly greater in height than that of the closed portion (1.872 × 0.872 inches). The difference in height is just the wall thickness (0.064 inches).

Because the waveguide is open, the fields fringe to the outside as shown in Fig. 9. Thus, to confine the fields to the medium, flanges of width w were added. The minimum width was determined experimentally for the case where the medium is free space (worst case). These flanges also have the advantage that the boundary value problem reduces from a three-media problem to a two-media problem, and is therefore more tractable analytically.

A typical plot of the detected signal is shown in Fig. 10. The field being scattered propagates as $\exp(-\gamma z)$, so phase sensitive detection gives an output

$$V_{out} = V_0 e^{-2\alpha z} \cos(2\beta z) \qquad (9)$$

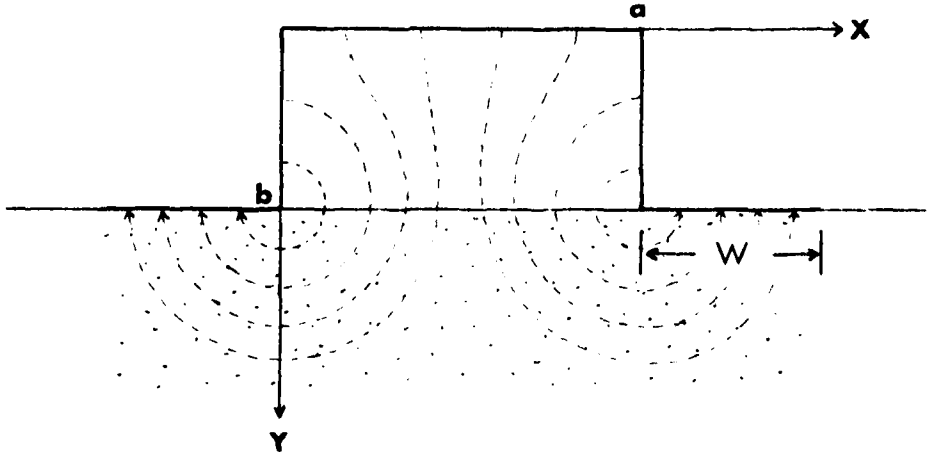

Fig. 9. Transverse electric field distribution of open-walled waveguide with flanges.

The attenuation constant α is easily calculated by measuring the slop (-2α) of the envelope of the peaks from the graph when plotted logarithmically (e.g., in dB). The phase constant β is $2\pi/\lambda$ where λ is the longitudinal wavelength in the guide, since the zero crossing occurs every quarter wavelength, β is easily obtained by measuring the distance between zero crossings. Again, greater accuracy is obtained by averaging over several zero crossings.

The complex propagation constant for various materials (rocks, concrete, sand, styrofoam, etc.) were measured and the results are shown in Fig. 11. It is evident that the various media have a significant effect on the attenuation, α, but the effect on the phase constant, β, is small. For reference, note that if the bottom wall is perfectly conducting (closed waveguide), $\alpha=0$ and $\beta=\beta_g$. The free space propagation constant, β_0, is also shown for reference.

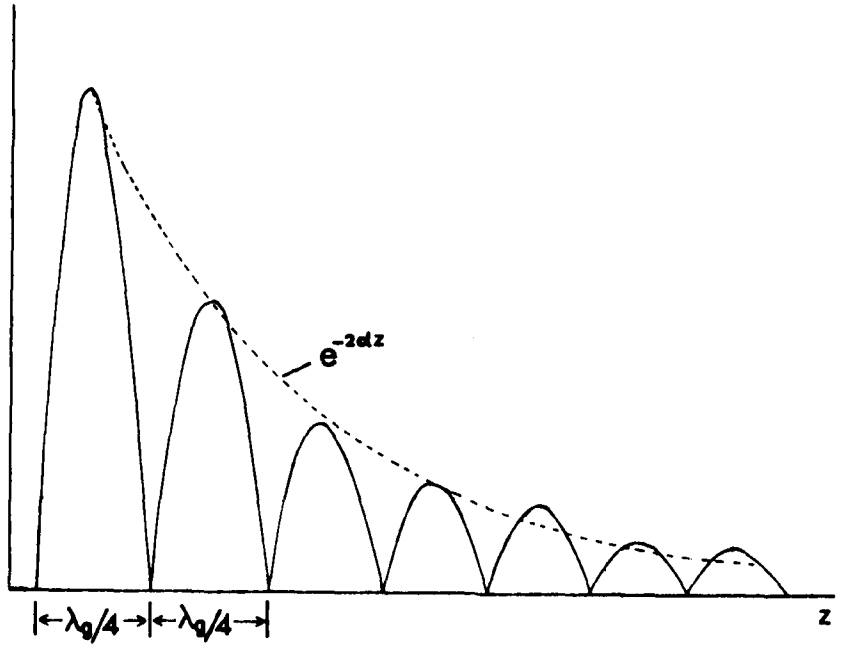

Fig. 10. Typical homodyne output for the non-invasive method.

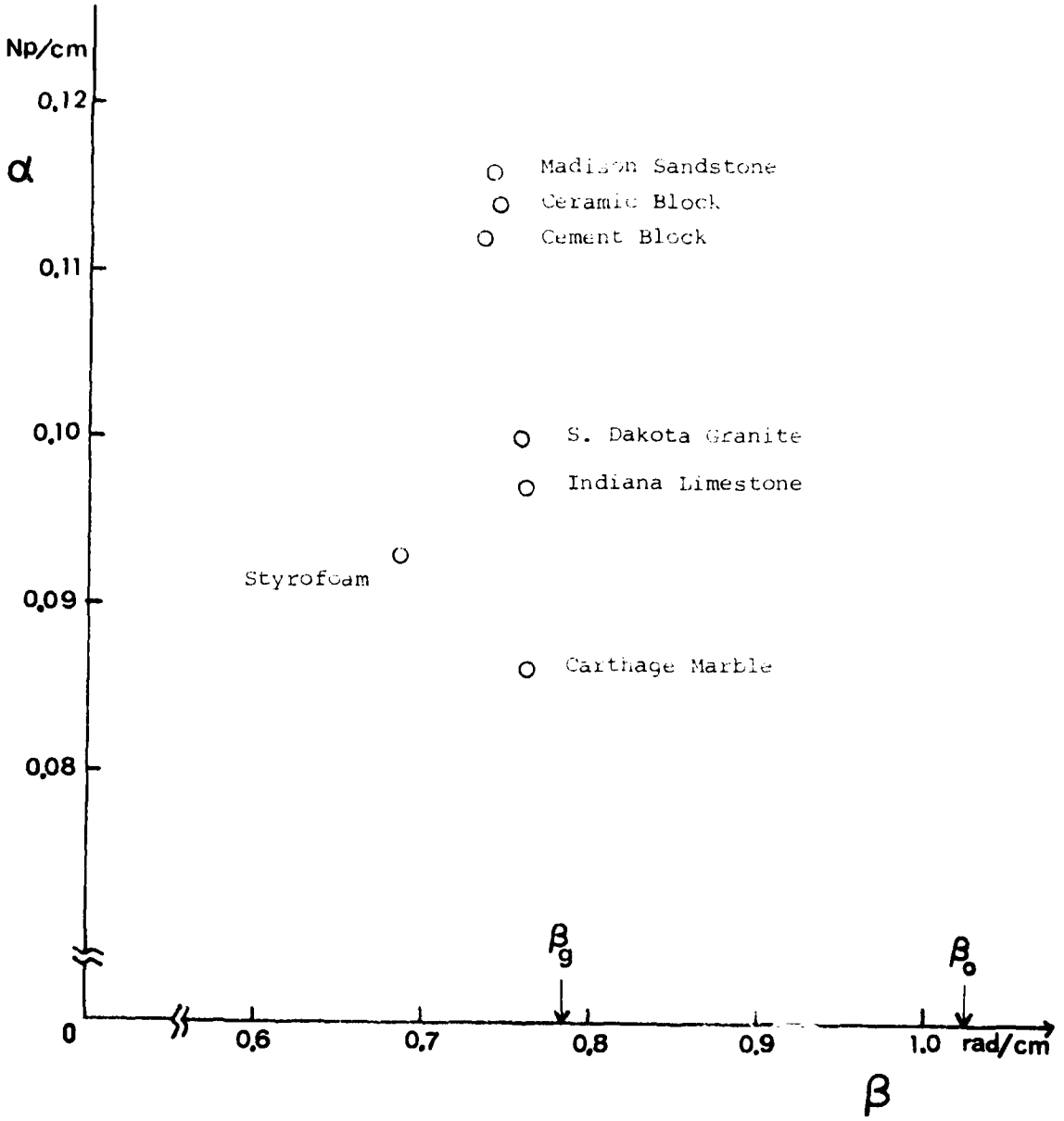

Fig. 11. Measured α and β values for various materials, using the instrumentation shown in Figs. 6-8.

III. FIELD ANALYSIS OF THE OPEN-WALLED WAVEGUIDE

1. Mode Configuration

To find the dielectric constant ε of the medium from the measured γ, the presence or absence of particular field (E and H) components must be known. This permits describing the wave with mode configurations suitable to an analytical study, i.e., solving the boundary value problem. The coordinate system is defined in Fig. 9.

First, the TE_x mode was tried. A "mode filter" in the form of an array of thin conducting wires in x-direction, spaced by 1 cm, was placed over the open side of the waveguide. This filter was intended to short out the E_x component at the aperture separating the interior of the waveguide and the exterior medium. As a result, E_x was reduced somewhat, but the measured α and β approached those of the closed waveguide signifying that the coupling to the medium was actually reduced. This is undesirable since the dependence on ε is reduced. Therefore, the TE_x mode analysis was superseded by the TM_y mode.

In general, any field can be decomposed into TM_y and TE_y modes. The TM_y mode has an E_y component while the TE_y mode does not. The TM_y mode in the open guide couples efficiently to the TE_z modes in the closed guide which only has a y-component of the electric field. Hence, the TM_y mode can be used to describe the field inside either the closed or open guide. It is unlikely that the TE_y mode even exists in the open guide since it is not excited by the E_y-component in the closed guide.

This argument is confirmed by measurement which shows large H_z versus x and virtually zero H_y as given in Fig. 12.

The scatterer used in this measurement was a small loop loaded with two tiny pill type PIN diodes electrically modulated and moved in the transverse direction via a nylon string.

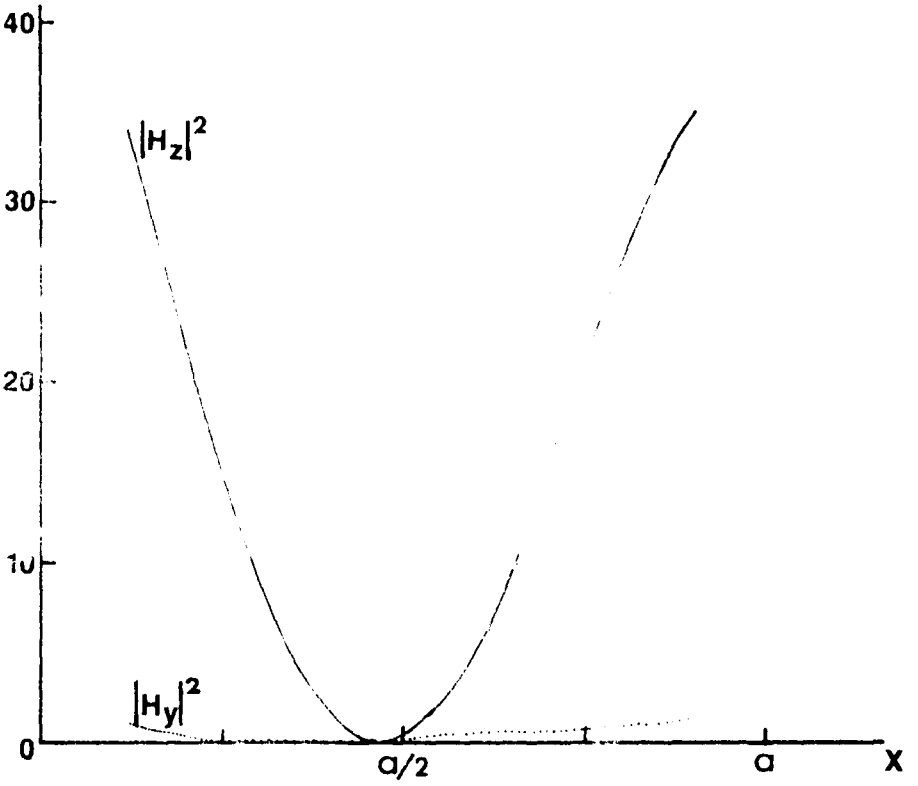

Fig. 12. Homodyne output for the magnetic field inside the open-walled waveguide at y = b/2.

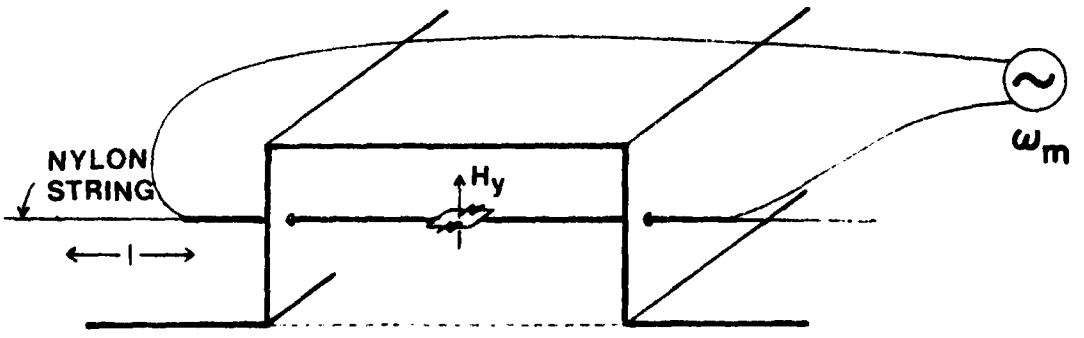

Fig. 13. Modulated scattering loop probe for measuring H_z and H_y inside the open waveguide.

We were unable to satisfactorily measure any of the electric field components (E_x, E_y or E_z) inside the open waveguide using an electric dipole. Coupling with the metal walls formed loops such that the results were strongly affected by the magnetic fields (H_x and H_z) rendering the results meaningless.

2. Field Analysis for the TM_y Mode

TM_y modes inside the open waveguide can be represented by a magnetic vector potential

$$\overline{A} = \overline{u}_y \psi$$

and

$$\overline{H} = \nabla \times \overline{A}$$

Then, the scalar wavefunction can be represented as

$$\psi(x,y,z) = \sum_{m=1}^{\infty} \frac{1}{2\pi} \sin\left(\frac{m\pi x}{a}\right) \int_0^{\infty} \Psi_m(k_y)\cos(k_y y)e^{-\gamma_m z}\, dk_y$$

$$= \sum_{m=1}^{\infty} \sin\left(\frac{m\pi x}{a}\right)\psi_m(y) \qquad (10)$$

for $z > 0$ and $0 < y < b$

where $$\Psi_m(k_y) = \int_0^{\infty} \psi_m(y)e^{-\gamma_m z}\cos(k_y y)\, dy \qquad (11)$$

is the cosine transform of $\psi_m(y)$. The dispersion relation is

$$k_0^2 - \left(\frac{m\pi}{a}\right)^2 - k_y^2 + \gamma_m^2 = 0 \qquad (12)$$

where $k_0^2 = \omega^2 \mu_0 \varepsilon_0$

The wavefunctions in (10) have been chosen to satisfy the boundary conditions on the three metal walls in the waveguide, i.e., $E_z = 0$ at x=0 and a, and y=0.

The fields inside the open waveguide are:

$$E_x = \frac{1}{j\omega\varepsilon_0} \frac{\partial^2 \psi}{\partial x \partial y}$$

$$= -\frac{1}{j\omega\varepsilon_0} \sum_{m=1}^{\infty} \frac{m}{2a} \cos\left(\frac{m\pi x}{a}\right) \int_0^{\infty} \psi_m(\rho_y) \sin(k_y y) e^{-\gamma_m z} \, dk_y \tag{13a}$$

$$E_z = \frac{1}{j\omega\varepsilon_0} \frac{\partial^2 \psi}{\partial y \partial z}$$

$$= \frac{1}{j\omega\varepsilon_0} \sum_{m=1}^{\infty} \frac{1}{2\pi} \sin\left(\frac{m\pi x}{a}\right) \int_0^{\infty} \psi_m(k_y) k_y \gamma_m \sin(k_y y) e^{-\gamma_m z} \, dk_y \tag{13b}$$

$$H_x = -\frac{\partial \psi}{\partial z}$$

$$= \sum_{m=1}^{\infty} \frac{1}{2\pi} \sin\left(\frac{m\pi x}{a}\right) \int_0^{\infty} \gamma_m \psi_m(k_y) \cos(k_y y) e^{-\gamma_m z} \, dk_y \tag{13c}$$

$$H_z = \frac{\partial \psi}{\partial x}$$

$$= \sum_{m=1}^{\infty} \frac{m}{2a} \cos\left(\frac{m\pi x}{a}\right) \int_0^{\infty} \psi_m(k_y) \cos(k_y y) e^{-\gamma_m z} \, dk_y \tag{13d}$$

The tactic is to find the fields outside the aperture and equate the tangential components at the aperture to determine the equivalent γ in terms of ε. To this end, apply the vector compensation theorem [Mittra, 1961], modified to the case where one source is located inside the perturbed region.

$$\int_{R_2} (\bar{J}_2 \cdot \bar{E}_1' - \bar{M}_2 \cdot \bar{H}_1')dV = \int_S (\bar{E}_1' \times \bar{H}_2 - \bar{E}_2 \times \bar{H}_1') \cdot d\bar{S} \qquad (14)$$

where the subscripts 1 and 2 denote the fields excited by the source 1 and source 2, respectively, and the primed fields are the perturbed fields whereas the unprimed ones are the unperturbed fields. We take the unperturbed state as a perfect electric conductor over the entire y=b plane.

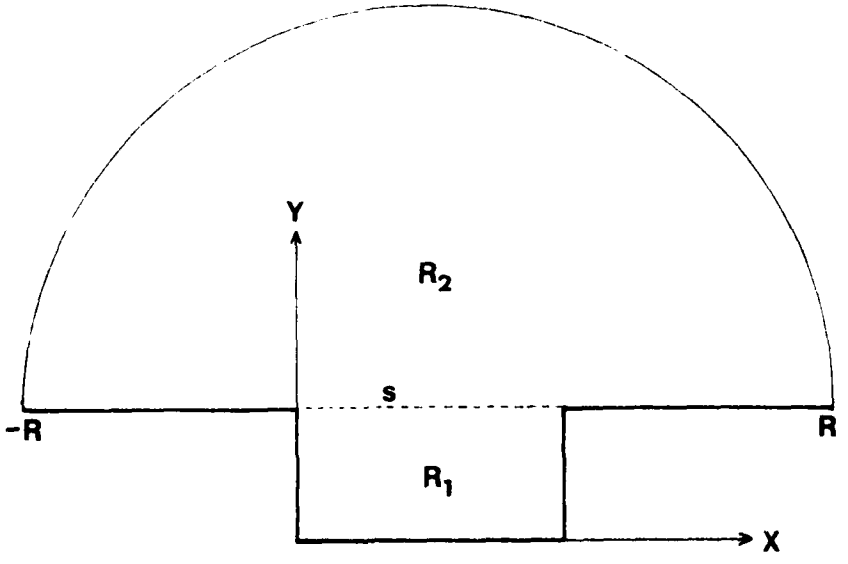

Fig. 14. Cross-section geometry of open-walled waveguide. In the unperturbed case, an electric conductor covers the aperture.

Next, put a uniform z-directed magnetic line source in R_2 in order to find H_{1z}'.

$$\bar{M}_2 = \bar{u}_z \, \delta(x-x')\delta(y-y')$$
$$\bar{J}_2 = 0$$

which excites TE_z fields with no z-variation. Thus (14) becomes

$$-\int_{R_2} \delta(x-x')\delta(y-y')H'_{1z}(x,y,z)dx\,dy\,dz = \int_S (\bar{E}'_1 \times \bar{H}_2 - \bar{E}_2 \times \bar{H}'_1) \cdot d\bar{S} \quad (15)$$

As $R \to \infty$ the RHS of (15) becomes the integration over entire y=b plane.

$$\int_{-\infty}^{\infty} H'_{1z}(x',y',z)dz = -\int_{-\infty}^{\infty} \{ \int_{-\infty}^{\infty} (\bar{E}'_1 \times \bar{H}_2 - \bar{E}_2 \times \bar{H}'_1)_{y=b} \cdot \bar{n}dx\}dz \quad (16)$$

For the unperturbed state $\bar{n} \times \bar{E}_2 = 0$ on y=b plane (perfect conducting plane), and for the perturbed state $\bar{n} \times \bar{E}'_1 = 0$ on y=b except over the aperture ($0 < x < a$ and $z > 0$). Therefore, (16) reduces to

$$\begin{aligned} \int_{-\infty}^{\infty} H'_{1z}(x',y',z)dz &= -\int_0^{\infty}\int_0^{a} (\bar{E}'_1 \times \bar{H}_2)_{y=b} \cdot \bar{u}_y\,dx\,dz \\ &= -\int_0^{\infty}\int_0^{a} (E'_{1x}H_{2z} - E'_{1z}H_{2x})_{y=b}\,dx\,dz \end{aligned} \quad (17)$$

The field excited by the z-directed magnetic line source is a TE_z mode. Thus,

$$H_{2x} = \frac{1}{j\omega\mu}\frac{\partial^2\psi^e}{\partial z \partial x}$$

Since there is no z-variation in ψ^e, $H_{2x} = 0$.

Moverover, H'_1 for $z < 0$ is the magnetic field of a diffracted wave. Thus for y'=b, $H'_{1z}(x',b,z)$ is small and decreases rapidly for $z < 0$. Hence, as a first approximation, neglect its contribution

$$\Delta_H = \int_{-\infty}^{0} H'_{1z}(x',b,z)dz \quad (18)$$

Then (17) becomes

$$\int_0^{\infty} H'_{1z}(x',b,z)dz \cong \int_0^{\infty}\int_0^{a} E'_{1x}(x,b,z)H_{2z}(x,b)dx\,dz \quad (19)$$

Both H'_{1z} and E'_{1z} have the same z-variation, but H_{2z} has no z-variation. Therefore,

$$H'_{1z}(x',b,z) = \int_0^a E'_{1x}(x,b,z)H_{2z}(x,b)dx \qquad (20)$$

The $H_{2z}(x,b)$ of the source at (x',b) can be found by using the potential function

$$\psi^e = \frac{1}{2j} H_0^{(2)}(k|x-x'|)$$

and

$$\bar{E} = -\nabla \times \bar{u}_z \psi^e$$

For the TE_z field of the line source

$$H_{2z} = \frac{1}{j\omega\mu} \left(\frac{\partial^2}{\partial z^2} + k^2\right)\psi^e$$

$$= -\frac{k^2}{2\omega\mu} H_0^{(2)}(k|x-x'|) \qquad (21)$$

Then, (20) becomes

$$H'_{1z}(x',b,z) = -\frac{k^2}{2\omega\mu} \int_0^a E'_{1x}(x,b,z)H_0^{(2)}(k|x-x'|)dx \qquad (22)$$

The surface impedance as seen looking from the waveguide into the medium is

$$Z_s = -\left.\frac{E'_{1x}}{H'_{1z}}\right|_{y=b} = \left.\frac{E'_{1z}}{H'_{1x}}\right|_{y=b} \qquad (23)$$

Put this relation into (16) and get

$$H'_{1z}(x',b,z) = \frac{k^2 Z_s}{2\omega\mu} \int_0^a H'_{1z}(x,b,z)H_0^{(2)}(k|x-x'|)dx \qquad (24)$$

From (13d) $H'_{1z}(x,y,z)$ inside the waveguide is

$$H'_{1z}(x,y,z) = \sum_{m=1}^{\infty} \frac{m}{2a} \cos\left(\frac{m\pi x}{a}\right) \int_0^{\infty} \psi_m(k_y) \cos(k_y y) e^{-\gamma_m z} dk_y$$

$$= \sum_{m=1}^{\infty} \frac{m\pi}{a} \cos\left(\frac{m\pi x}{a}\right) \psi_m(y) \qquad (25)$$

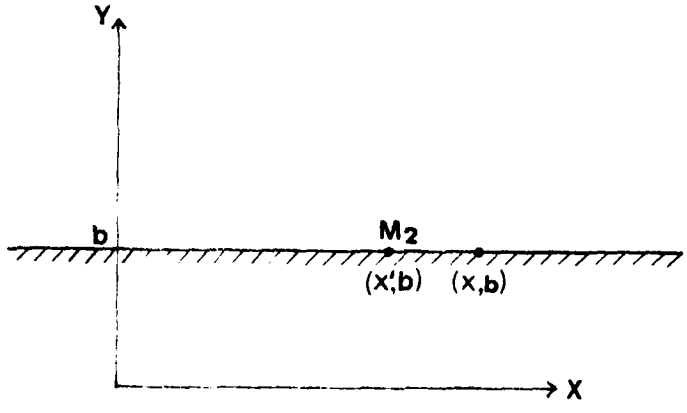

Fig. 15. Geometry of unperturbed problem for determining H_{2z}.

Thus, equating the tangential magnetic fields (24) and (25) at the aperture,

$$\sum_{m=1}^{\infty} \frac{m\pi}{a} \cos\left(\frac{m\pi x'}{a}\right) \psi_m(b) = \frac{k^2 Z_s}{2\omega\mu} \int_0^a \sum_{m=1}^{\infty} \frac{m\pi}{a} \cos\left(\frac{m\pi x}{a}\right) \psi_m(b) H_0^{(2)}(k|x-x'|)dx$$

$$= \sum_{m=1}^{\infty} \frac{m\pi}{a} \psi_m(b) \frac{k^2 Z_s}{2\omega\mu} \int_0^a \cos\left(\frac{m\pi x}{a}\right) H_0^{(2)}(k|x-x'|)dx \qquad (26)$$

Equating term-by-term for each m,

$$\cos\left(\frac{m\pi x'}{a}\right) = \frac{k^2 Z_s}{2\omega\mu} \int_0^a \cos\left(\frac{m\pi x}{a}\right) H_0^{(2)}(k|x-x'|)dx \qquad (27)$$

Now, E'_{1z} is also needed in order to find the complete tangential fields at the aperture. This makes the solution unique. The process can be repeated for the unperturbed problem where source 2 is a uniform electric line current and a perfect magnetic conducting strip covers $0 < x < a$ and $-\infty < z < +\infty$. Then remove the perfect magnetic conducting strip to form the perturbed problem.

Let $\bar{J}_2 = \bar{u}_z \delta(x-x')\delta(y-y')$

$\bar{M}_2 = 0$

which excites a TM_z field with no z-variation.

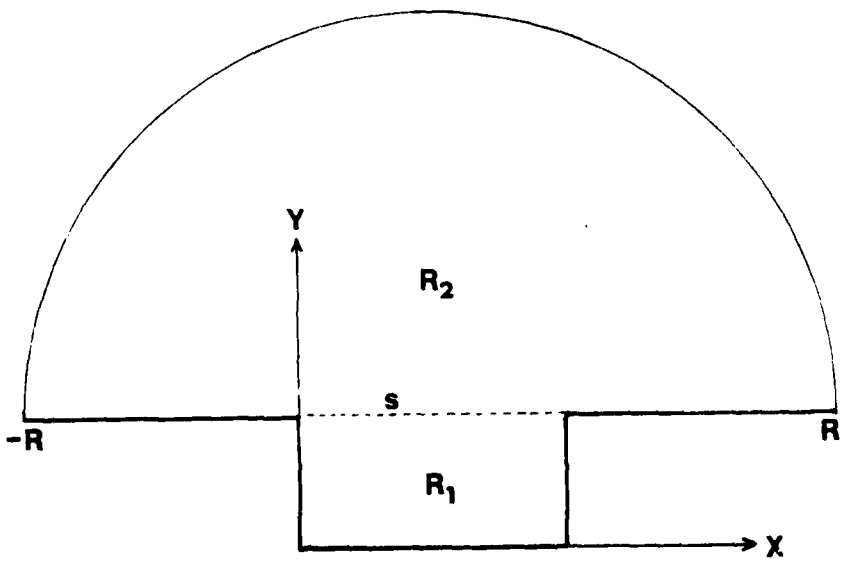

Fig. 16. Geometry of the unperturbed problem. A magnetic conducting strip extends $-\infty < z < +\infty$.

Then, (14) becomes

$$\int_{-\infty}^{\infty} E'_{1z}(x',y',z)dz = -\int_{-\infty}^{\infty} \{ \int_{0}^{a} (\bar{E}_2 \times \bar{H}'_1)_{y=b} \cdot \bar{u}_y dx \} dz \qquad (28)$$

since H_2 has no tangential component on the magnetic conductor which covers the aperture and E'_1 has no tangential component on the perfect electric conductors at the sides of the aperture.

Also, for the TM_z mode

$$E_x = \frac{1}{j\omega\epsilon} \frac{\partial^2 \psi^h}{\partial x \partial z}$$

and since there is no z-variation, E_{2x} vanishes. Furthermore, $E'_{1z}(x',b,z)$ also vanishes for $z < 0$, H'_{1x} is a small diffracted field for $z < 0$. Hence, (28) becomes

$$\int_0^\infty E'_{1z}(x',b,z)dz \cong -\int_0^\infty \left\{ \int_0^a E_{2z}(x,b)H'_{1x}(x,b,z)dx \right\} dz \qquad (29)$$

Both E'_{1z} and H'_{1x} have the same z-variation, but E_{2z} has no z-variation. Thus,

$$E'_{1z}(x',b,z) = -\int_0^a E_{2z}(x,b)H'_{1x}(x,b,z)dx \qquad (30)$$

From (23)

$$H'_{1x}(x,b,z) = \frac{1}{Z_s} E'_{1z}(x,b,z)$$

Therefore,

$$E'_{1z}(x',b,z) = -\int_0^a \frac{1}{Z_s} E'_{1z}(x,b,z)E_{2z}(x,b)dx \qquad (31)$$

From (13b)

$$E'_{1z}(x,y,z) = \frac{1}{j\omega\epsilon_0} \sum_{m=1}^{\infty} \sin\left(\frac{m\pi x}{a}\right) \frac{1}{2\pi} \int_0^\infty \psi_m(k_y) e^{-\gamma_m z} k_y \gamma_m \sin(k_y y)dk_y$$

$$= \frac{1}{j\omega\epsilon_0} \sum_{m=1}^{\infty} \sin\left(\frac{m\pi x}{a}\right) \frac{\partial^2}{\partial y \partial z} \psi_m(y) \qquad (32)$$

Hence, (31) becomes

$$\frac{1}{j\omega\epsilon_0} \sum_{m=1}^{\infty} \sin\left(\frac{m\pi x'}{a}\right) \frac{\partial^2}{\partial y \partial z} \psi_m(y)\Big|_{y=b}$$

$$= -\int_0^a \frac{1}{j\omega\epsilon_0 Z_s} \sum_{m=1}^{\infty} \sin\left(\frac{m\pi x}{a}\right) \frac{\partial^2}{\partial y \partial z} \psi_m(y)\Big|_{y=b} E_{2z}(x,b)dx \qquad (33)$$

Equating term-by-term for each m,

$$\sin\left(\frac{m\pi x'}{a}\right) = -\int_0^a \frac{1}{Z_s} \sin\left(\frac{m\pi x}{a}\right) E_{2z}(x,b)\,dx \qquad (34)$$

(a) (b)

Fig. 17. (a) Geometry for the unperturbed problem
(b) Approximation of (a).

As a first aproximation to find E_{2z}, the fields on the magnetic strip laid on an electrically conducting plane is approximated by the fields on a perfect magnetic conductor plane (Fig. 17). Then $E_{2z}(x,b)$ of the source at (x',b) can be found using the potential function

$$\psi^h = \frac{1}{2j} H_0^{(2)}(k|x-x'|) \qquad (35)$$

and

$$\overline{H} = \nabla \times \overline{u}_z \psi^h$$

For TM_z fields,

$$\overline{E}_z = \frac{1}{j\omega\varepsilon}\left(\frac{\partial^2}{\partial z^2} + k^2\right)\psi^h$$

so

$$E_{2z}(x,b) = -\frac{k^2}{2\omega\varepsilon} H_0^{(2)}(k|x-x'|) \qquad (36)$$

Thus, (34) becomes

$$\sin\left(\frac{m\pi x'}{a}\right) = \frac{k^2}{2\omega\epsilon} \int_0^a \frac{1}{Z_s} \sin\left(\frac{m\pi x}{a}\right) H_0^{(2)}(k|x-x'|)dx$$

$$\simeq \frac{k^2}{2\omega\epsilon Z_s} \int_0^a \sin\left(\frac{m\pi x}{a}\right) H_0^{(2)}(k|x-x'|)dx \qquad (37)$$

The equations (27) and (37) give a set of simultaneous equations. Their sum gives

$$\frac{\mu}{Z_s} \cos\left(\frac{m\pi x'}{a}\right) + jZ_s\epsilon \sin\left(\frac{m\pi x'}{a}\right) = \frac{k^2}{2\omega} \int_0^a e^{\frac{jm\pi x}{a}} H_0^{(2)}(k|x-x'|)dx \qquad (38)$$

To remove the dependence on x', integrate both sides of (38) over x' from 0 to a.

$$j\frac{2a}{m\pi} Z_s\epsilon = \frac{k^2}{2\omega} \int_0^a \int_0^a e^{\frac{jm\pi x}{a}} H_0^{(2)}(k|x-x'|)dx\,dx' \qquad (39)$$

for $m = 1, 3, 5 \ldots$.

The surface impedance Z_s as seen looking into the medium is given by

$$Z_s = \left.\frac{E'_{1z}}{H'_{1x}}\right|_{y=b}$$

and using (13b) and (13c),

$$= \frac{1}{j\omega\epsilon_0} \left.\frac{\sum_{m=1}^{\infty} \sin\left(\frac{m\pi x}{a}\right) \frac{\partial^2\psi_m(y)}{\partial y\partial z}}{-\sum_{m=1}^{\infty} \sin\left(\frac{m\pi x}{a}\right) \frac{\partial\psi_m(y)}{\partial z}}\right|_{y=b} \qquad (40)$$

As an alternative, the surface impedance for each m th mode can be defined

$$Z_{sm} = -\frac{1}{j\omega\varepsilon_0} \left. \frac{\frac{\partial^2}{\partial y \partial z}\psi_m(y)}{\frac{\partial}{\partial z}\psi_m(y)} \right|_{y=b} \tag{41}$$

Assume that the m=1 mode is predominant in the open-walled waveguide. Then, $Z_s \cong Z_{s1}$ and assume that

$$\psi_1(y) \cong A \cos(k_{y1}y)\, e^{-\gamma_1 z} \tag{42}$$

where k_{y1} is complex.

Then,

$$Z_s \cong \frac{1}{j\omega\varepsilon_0} k_{y1} \tan(k_{y1}b) \tag{43}$$

Finally, (39) becomes

$$k_{y1} \tan(k_{y1}b) = \frac{\pi k_0^2}{4a} \int_0^a \int_0^a e^{\frac{j\pi x}{a}} H_0^{(2)}(k|x-x'|)dx\, dx' \tag{44}$$

This final equation has a Hankel function with complex argument in its integrand, so numerical methods must be used to solve it for k_{y1}. Then γ_1 is

$$\gamma_1 = \sqrt{(\tfrac{\pi}{a})^2 + k_{y1}^2 - k_0^2}$$

and, by the assumptions previously taken

$$\gamma \cong \gamma_1$$

Solving (44) for ε_r from the measured γ is very difficult and takes much computing time. However, computing γ from assumed values of ε_r is relatively simple. It is then possible to plot a map of ε_r as a function of γ as shown in Fig. 18. Some of the measured γ's shown in Fig. 11 are also shown.

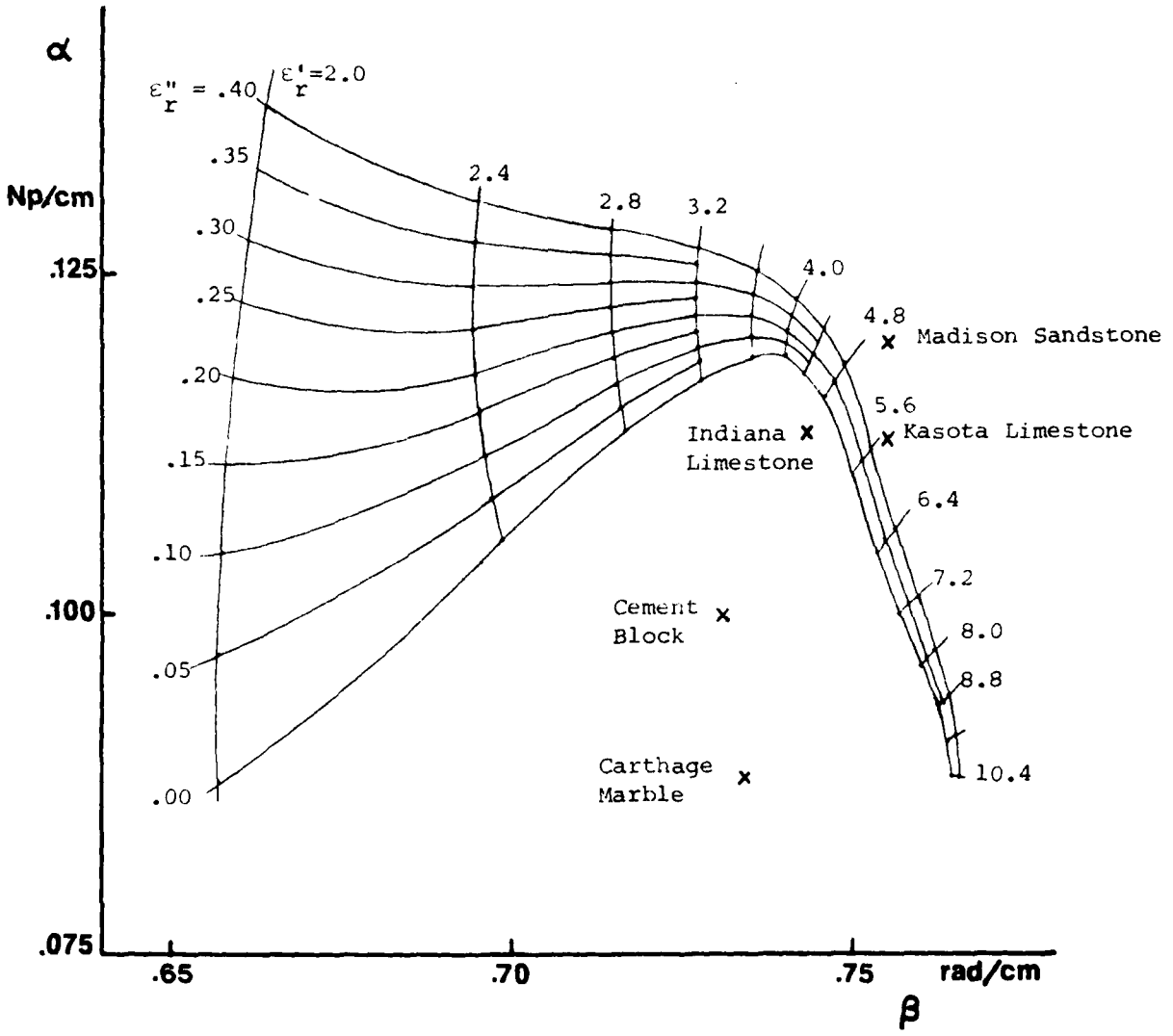

Fig. 18. Results of numerical solution of (44).

IV. DISCUSSION

The three data points which are located below the $\varepsilon_r'' = 0$ curve in Fig. 18 do not fit well, since ε_r'' is negative (as $\varepsilon_r = \varepsilon_r' - j\varepsilon_r''$, both ε_r' and ε_r'' should be positive). The probable reason for the discord of the numerical and experimental results is that the approximations taken in the theory are too rough, especially in the assumed field in the unperturbed state, (36). For a better approximation, the original situation of Fig. 17(a) can be approximated by removing the magnetic strip and replacing the source with a source of 2J (original source plus its image) situated between two thin electrically conducting half-planes as shown in Fig. 19.

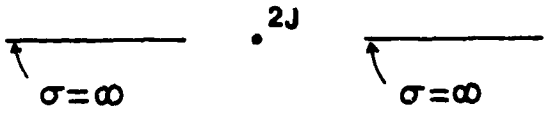

Fig. 19. Approximated problem for Fig. 17(a).

In this case the potential function of the form

$$\psi^h = \frac{1}{2j} \sum_{m=1}^{\infty} \psi_m \sin\left(\frac{m\pi x}{a}\right) H_0^{(2)}(k|x-x'|) \qquad (45)$$

should be tried instead of (35). This function satisfies the boundary conditions at the both edges, x=0 and x=a, of the conducting half planes. Again, the m=1 mode would be dominant. Hence,

$$\psi^h \simeq \frac{1}{2j} \sin\left(\frac{\pi x}{a}\right) H_0^{(2)}(k|x-x'|) \qquad (46)$$

So instead of (36), a better approximation to the unperturbed field is

$$E_{2z}(x,b) = -\frac{k^2}{2\omega\varepsilon} \sin(\frac{\pi x}{a}) H_0^{(2)}(k|x-x'|) \qquad (47)$$

And finally, (44) would be replaced by

$$k_{y1} \tan(k_{y1}b) = j \frac{\pi k_0^2}{4a} \int_0^a \int_0^a \sin^2(\frac{\pi x}{a}) H_0^{(2)}(k|x-x'|)dx\, dx' \qquad (48)$$

which should improve the results significantly.

Another problem is that the computed γ's are concentrated in a narrow strip for $\varepsilon_r' > 4.0$. This characteristic makes it difficult to accurately find ε from the measured γ, even if the theory is correct. We believe that this difficulty can be overcome by filling the waveguide with a low-loss dielectric material with $\varepsilon_r' = 4$ to 6. Introducing such a dielectric in the system will scale down the ε_r of the material relative to that inside the waveguide. This would make the most of γ's fall in the wide-spread region of the map. Conversion to the system to use a dielectric-filled waveguide is planned.

V. FUTURE STUDIES

The accuracy in measuring α can be substantially increased by using a "phase-insensitive homodyne detector" used by King and Yen [1981] which is similar to a quadrature SSB modulator with output of the form

$$K_h|b|m\cos(\omega_m t+\phi)$$

instead of

$$K_h|b|m\cos(\phi)\cos(\omega_m t)$$

as in (2). Hence, a continuous variation of $|b|$ can be measured to determine α in the phase-insensitive system, while only several peaks of the output are used in the conventional phase-sensitive system as seen in Fig. 10.

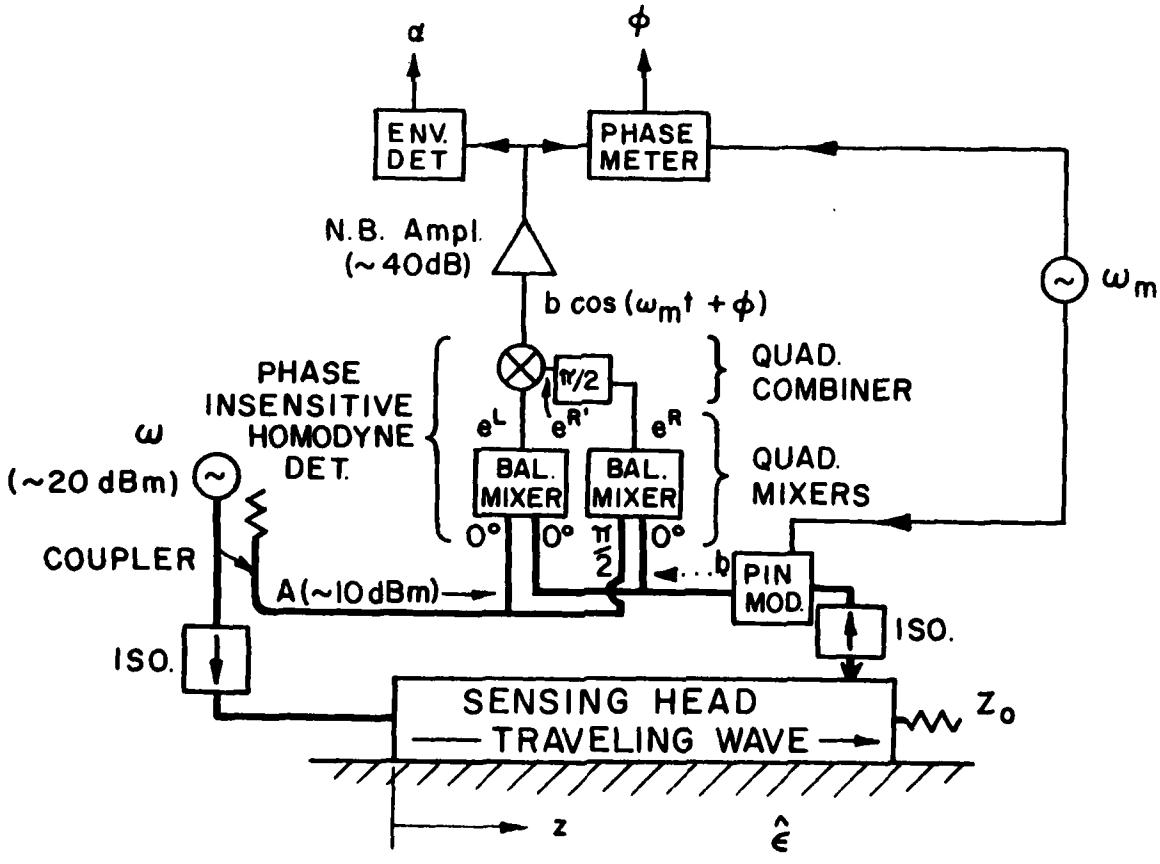

Fig. 20. Phase-insensitive homodyne system.

Moreover, this phase-insensitive system detects one-way transmission of the signal

$$b = b_0 e^{-\alpha z} e^{-j\beta z}$$

rather than the round-trip backscattered signal. Thus, this system is twice as sensitive (as measured in dB). In this system the phase βz is measured by a phase meter.

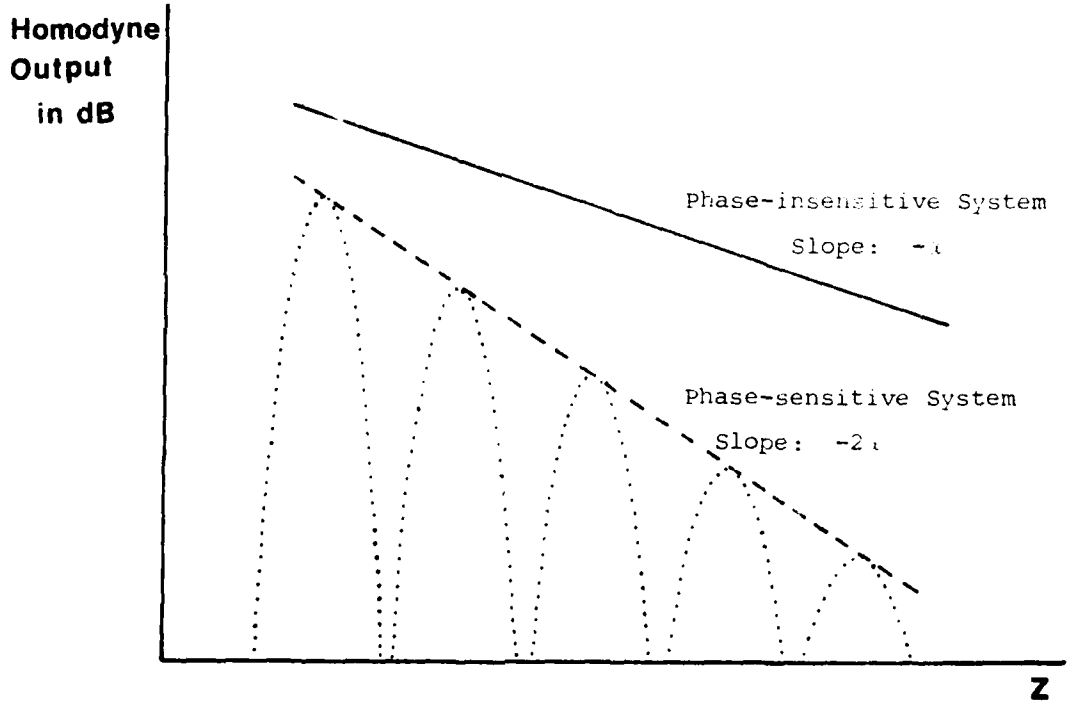

Fig. 21. Comparison of the outputs of phase-insensitive system and phase-sensitive systems.

Both the invasive and the non-invasive methods used have some difficulties. However, most of them can be reduced using different devices for coupling the fields to the medium.

For the invasive method, the surface wave launching arrangement shown in Fig. 22 has several advantages over that shown in Fig. 2.

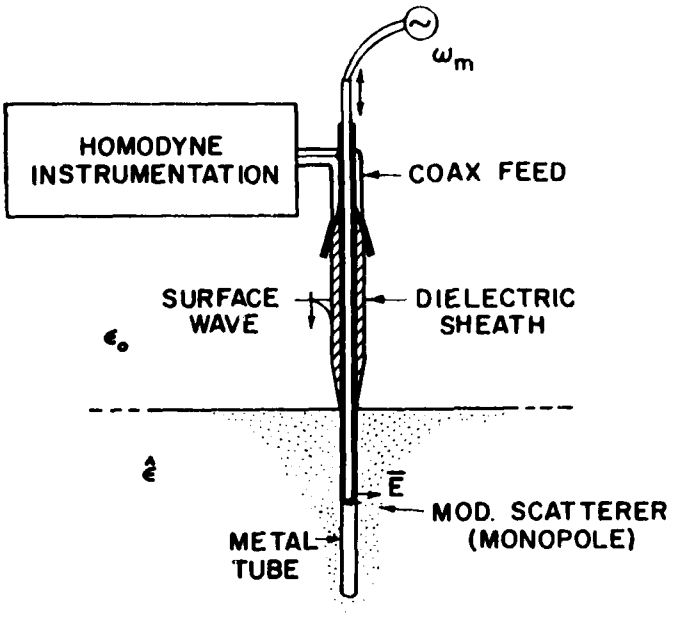

Fig. 22. New invasive surface wave structure.

The microwave instrumentation is rigidly attached to a coaxial line which feeds a surface wave structure through a tapered transition. The surface wave structure consists of a dielectric sheath on the stationary metal tube. The sheath is terminated with a gradual taper just above the medium interface, and the metal tube intrudes to a depth of about 2λ into the medium. A modulated monopole scatterer mounted at the end of a plastic tube is inserted into the metal tube, extending into the medium through a slot cut in the metal tube. Modulation of the PIN diode terminating the scatterer is accomplished by leads running through the plastic tube to an external AF oscillator.

Advantages of this new system are that:

a) The surface wave structure tends to focus the radiation into the medium along the metal tube so that the field intensity is greater than for the old system in Fig. 2.

b) The microwave source is a rigid integral part of the probing mechanism.

c) A monopole more nearly probes the field at a point (in contrast to the area of a loop). It is easier to tune, and the scattered field is generally larger.

d) The leads being used to modulate the PIN diode are shielded by the metal tube.

e) The operating frequency range is much broader than for the old system. The upper frequency limit is determined by the presence of higher order modes propagating on the surface waveguide, and the lower frequency limit is generally determined by the insertion length of the metal tube ($\sim 2\lambda$), and the system sensitivity.

For the non-invasive method the open-walled rectangular waveguide has a very limited operating frequency range. Approximately, this range corresponds to cutoff for the dominant TE_{10} mode of a closed waveguide at the low end, and to cutoff of the next higher order mode at the high end. The split rigid coaxial line in Fig. 23 has a cut off frequency of zero. This considerably extends the lower end of the frequency range until the physical size limitation is reached (again, approximately 2λ).

Another suggested non-invasive method uses coplanar strip lines laid directly on the medium to measure the propagation constant of a quasi-TEM wave. Its configuration is shown in Fig. 24. Since there are two conductors and two dielectrics (air and the medium), the dominant mode is quasi-TEM. Therefore, its cut off frequency is zero. The lower end of the usable

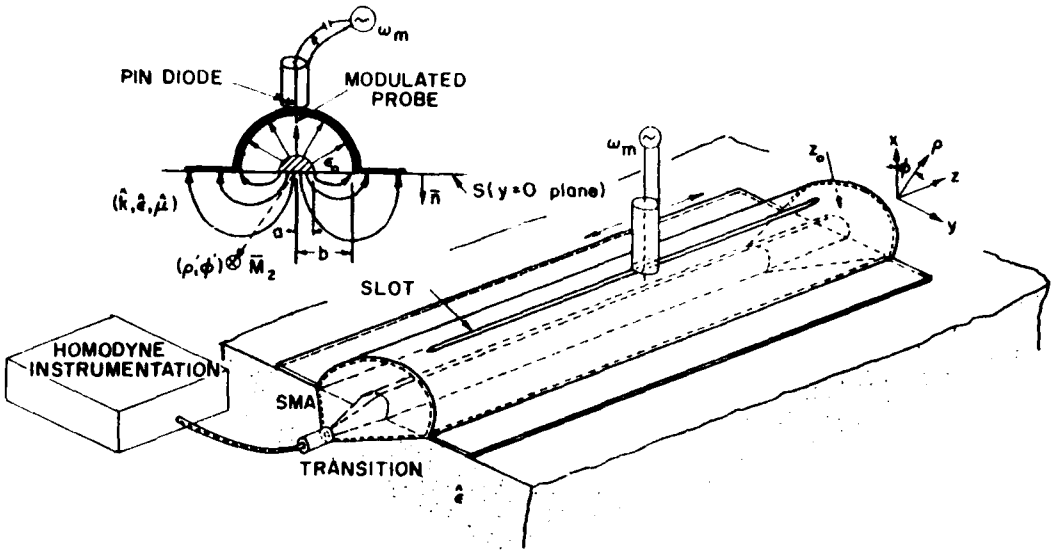

Fig. 23. Split coaxial line traveling wave sensing head.

bandwidth will chiefly be determined by the length of the strip lines. The higher end will be determined by appearance of any higher order modes. Hence this method gives a wide operating frequency range.

Another advantage of this method is that it can adapt to a slowly varying uneven surface. The coupling of the wave to the medium can be increased by increasing the width of the gap between the two conductors. Wide conductors also enhance the coupling and can reduce the effect of surface roughness as suggested by Chang and Wait [1974].

The coplanar strip line can be fed using a semi-rigid coaxial line by grounding the shield to one strip and the extended center conductor to other strip, as shown in Fig. 24. The line can be terminated in Z_0 over a broad range of frequencies using an electric and/or magnetic absorbing wedge.

The modulated scattering probe can be either an electric monopole or magnetic dipole, terminated in a PIN diode which is switched at ω_m. The probe can be moved along the line to measure α and β of the traveling wave.

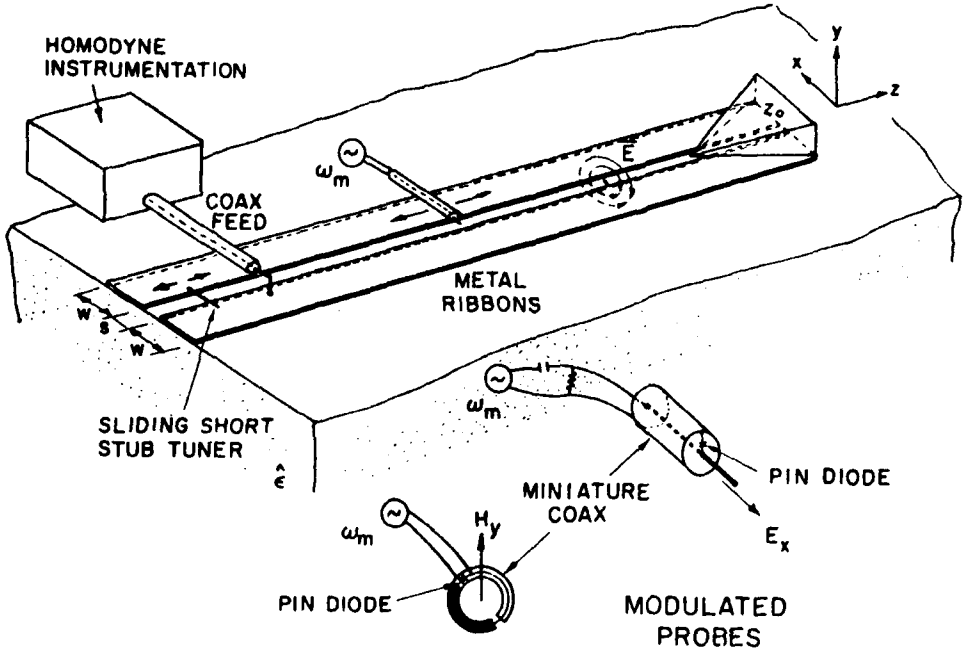

Fig. 24. Coplanar strip line traveling wave sensing head.

For a half-buried round wire, Chang and Wait found that

$$\frac{\gamma}{j\beta_0} = \left[\frac{1+\epsilon_r}{2}\right]^{1/2}$$

which means that the effective dielectric constant is the average of the two half-spaces. It is expected to that the measured γ will have fairly strong dependence on ϵ_r of the medium which promises more accurate measurement of ϵ_r.

VI. SCIENTIFIC PERSONNEL

Ray J. King, Professor and Principal Investigator

James B. Beyer, Professor and Co-Investigator

Chul Dong Kim, Research Assistant and Ph.D. Candidate

REFERENCES

Chang, D. C. and J. R. Wait, "Extremely Low Frequency (ELF) Propagation Along a Horizontal Wire Located Above or Buried in the Earth," IEEE Trans., COM-22(4), pp. 421-426, April, 1974.

Gardoil, F. E., "Slotted Line Measurements for Propagation Constant in Lossy Waveguide," IEEE Trans., MTT-23(3), pp. 317-319, March,1975.

King, R. J., Microwave Homodyne Systems, London: Peter Peregrinus Press, 1978.

King, R. J. and Y. H. Yen, "Probing Amplitude, Phase and Polarization of Microwave Field Distributions in Real-Time," IEEE Trans., MTT-29(11), pp. 1225-1231, Nov. 1981.

Mittra, R., "A Vector Form of Compensation Theorem and Its Application to Boundary-Value Problems," Dept. of Elec. Eng., University of Colorado, Boulder, CO, Sci. Report 2, AFCRL 575, June 15, 1961.


FILMED
8